Herrn Professor Dr H. Schröcke, München, danke ich vielmals für die Darstellung der beiden Proben. Weiterhin danke ich der Gesellschaft für Kernforschung, Karlsruhe, Abteilung RBT/KTB, für die Bereitstellung des Strahlrohres und eines Arbeitsplatzes am Reaktor FR2 sowie dem Bundesministerium für Forschung und Technologie für finanzielle Unterstützung.

Literatur

BAYER, G. (1962). *Ber. Dtsch. Keram. Ges.* **39**, 535–554.
BAYER, G. (1965). *U. S. Patent Office* 3, 165, 419, 2 S.
BIRSS, R. R. (1966). *Symmetry and Magnetism.* Amsterdam: North Holland.
GALY, J. & SENEGAS, J. (1972). *C. R. Acad. Sci. Paris. Sér. C*, **275**, 665–668.
HOLMES, L. M., BALLMAN, A. A. & HECKER, R. R. (1972). *Solid State Commun.* **11**, 409–413.
KLEIN, S. & WEITZEL, H. (1975). *J. Appl. Cryst.* **8**, 54–59.
KLEIN, S. & WEITZEL, H. (1976). *Acta Cryst.* A**32**, 587–591.
KOPTSIK, V. A. (1966). *Schubnikow Gruppen.* (In Russisch). Moskau: Izd. MGU.
KOZMANOV, YU. D. (1957). *Zh. Fiz. Khim.* **31**, 1861–1865.
PARANT, C., BERNIER, J. C. & MICHEL, A. (1973). *C. R. Acad. Sci. Paris, Sér. C*, **276**, 495–497.
SENEGAS, J. & GALY, J. (1974). *J. Solid State Chem.* **10**, 5–11.
SHULL, C. G., STRAUSER, W. A. & WOLLAN, E. O. (1951), *Phys. Rev.* **83**, 333–345.
TRUNOV, V. K. & KOVBA, L. M. (1966). *Izv. Akad. Nauk SSSR, Neorg. Mater.* (Engl. Übers.). **2**, 127–130.
WEITZEL, H. (1971). *Z. anorg. allgem. Chem.* **380**, 119–127.
WEITZEL, H. & KLEIN, S. (1973). *Solid State Commun.* **12**, 113–116.
WEITZEL, H. & KLEIN, S. (1974). *Acta Cryst.* A**30**, 380–384.

Acta Cryst. (1976). A**32**, 597

A Structural Study of the Alloy Cu_3Au above its Critical Temperature

BY P. BARDHAN* AND J. B. COHEN

Department of Materials Science and Engineering, The Technological Institute, Northwestern University, Evanston, Illinois 60201, *U.S.A.*

(*Received* 6 *October* 1975; *accepted* 24 *December* 1975)

Absolute measurements of the diffuse intensity in a volume in reciprocal space have been made at six temperatures ranging from 2°C above T_c to 930°C. The Warren short-range order parameters were obtained after correcting for the intensity due to atomic displacements in a more complete manner than in earlier studies. As a result the short-range order parameters are considerably smaller than in these earlier investigations. The (previously disputed) specific heat anomalies in Cu_3Au above T_c and the $L1_2$ phase have been shown to be associated with unusual changes in diffuse X-ray scattering *vs* temperature. From studies of the scattering distributions, computer simulation and pair potentials obtained with the Warren short-range order parameters, the anomaly at 600°C appears to be due to the disappearance of DO_{22}-like fluctuations, whereas above 850°C, CuPt-like fluctuations develop. There are premonitory effects just above T_c; there is a large increase in the Debye–Waller factor, in the total intensity due to quadratic terms in atomic displacements, and an apparent change in the sign of average first-neighbor displacement. The long-range oscillations in the interatomic potentials determined from the diffuse-scattering data fit the Friedel potential *only* approximately. The electron-to-atom ratio in Cu_3Au was found to be $\sim 0{\cdot}97$, in agreement with results on Cu alloys by other methods.

Introduction

The development of long-range order in the alloy Cu_3Au as it transforms from the $A1$ to the $L1_2$ structure is one of the classical examples of a first-order phase transition. There is increased interest in the nature of such phase changes and in particular in any precursory phenomena, which can lead to an understanding of the nature of atomic motions in the transition itself. Despite the extensive literature on this alloy very little information is available on the structure just above its critical temperature (T_c). X-ray diffraction studies have been made by Wilchinsky (1944) on quenched powders, and by Cowley (1950*a*, *b*) and Moss (1964) on single crystals held at temperature. The temperatures involved ranged from 405°C (about 10°C above T_c) to 750°C, whereas the melting point is about 950°C. Thus there is no information very close to T_c, nor does the available data extend over the entire temperature range. Yet measurements in the literature indicate anomalies in specific heat (Kuczynski, Doyama & Fine, 1956; Guarini & Schiavini, 1965) and other properties (Damask, Fuhrman & Germagnoli, 1961; Benci, Gasparrini & Germagnoli, 1964; Feder & No-

* Presently Postdoctoral Research Fellow, Department of Metallurgy, University of Newcastle, Newcastle-upon-Tyne, England.

wick, 1955; Dugdale, 1956; Schüle, 1957) at approximately 600 and 850 °C. While these have been questioned by Hirabayashi, Nagasaki and Kono (1957), who suggested that the effects were due to quenching, they used a much faster heating rate than the others; the sheer body of evidence by several workers whose data was taken at high temperatures strongly suggests that there may well be some abrupt changes in the solid solution, rather than just a steady decrease in short-range order with increasing temperature above T_c. Similar anomalies have been reported for Cu_3Zn (Masumoto, Saito & Sergihara, 1952) and Cu_3Pt (Bidwell, Schulz & Saxer, 1967). The only X-ray measurement on Cu_3Au that bracketed these temperatures was by Borie & Warren (1956) on a quenched single crystal, but this study did not reveal any dramatic changes.

An expansion of the free energy of this material in terms of some long-range order parameter must contain odd powers because the phase change is first order; in other words free energy *versus* order must resemble Fig. 1 just above T_c. [There may, in fact, be several order parameters so that such a figure should be drawn in a multidimensional space.] The presence of one or more subsidiary minima in this curve implies that there could be – indeed should be – long-lived fluctuations above the critical temperature whose nature could change with temperature if the relative positions of the minima also change. It is just such a concept that is involved in one current interpretation of the formation of the omega phase in Ti and Zr alloys (Cook, 1974).

In addition to the sparsity of structural information above T_c for Cu_3Au there are some technical problems with the available data. There are significant contributions to the diffuse scattering due to static displacements from lattice sites which arise from the differences in atomic size of the Cu and Au atoms, and this has not been adequately accounted for in previous studies. Wilchinsky attempted no correction. Cowley symmetrized his data (Moss & Clapp, 1968) and corrected for thermal diffuse scattering using a partially ordered single crystal. Moss corrected for thermal diffuse scattering in a similar manner, allowed for a temperature correction of the diffuse intensity and took into account only the nearest neighbor average static displacements, not more distant terms nor mean-square displacements. The latter diffuse intensity peaks at Bragg reflections and is known as the Huang (1947) effect. The scattering due to thermal vibrations also is largest near Bragg peaks. But there is appreciable scattering from both effects far from the peaks.

There have also been some studies at high temperatures by electron diffraction (Raether, 1952; Marcinkowski & Zwell, 1963; Hashimoto & Ogawa, 1970). These have been qualitative in nature but have made an important contribution by showing that the diffuse intensity above T_c was not peaked near the superlattice reflections of the $L1_2$ phase but consisted of diffuse satellites near these positions. [This was subsequently found with X-rays by Moss (1965).] It appears from these studies that this form of the intensity may be due to the shape of the Fermi surface and thus arises from long-range interactions (Moss, 1969), but see below.

The investigation to be reported here involved studies with a single crystal of the diffuse scattering in absolute units in a volume of reciprocal space at six temperatures from 2 °C above T_c to 930 °C, and at intermediate temperatures to bracket the specific heat anomalies. The scattering due to local order and that due to atomic displacements have been separated more completely than heretofore.

Qualitative observations are reported on the atomic displacements and these are correlated with the local order. A quantitative analysis of the data in terms of the Warren short-range order parameters provided direct information on the atomic configurations and interaction energies.

Experimental procedures

The X-ray diffractometer employed in this study was a modified G.E. XRD-5 unit (Schwartz, Morrison & Cohen, 1963), equipped with an incident beam, doubly-bent pyrolitic graphite monochromator. Co $K\alpha$ radiation (50 kV, 6 mA) was employed with a scintillation counter and pulse height analyzer. Total horizontal divergence was 1·6° and total vertical divergence was 2·6° and the tails of the incident beam were carefully reduced with slits. These divergences correspond to an uncertainty in reciprocal space in the region explored of $\Delta h \simeq 0{\cdot}06$–$0{\cdot}09$. To hold counting precision to within statistical errors for a week or more, counts were measured *vs* those to a second detector measuring the fluorescence from a cellophane film containing VO powder and placed in the beam between monochromator and crystal. The polarization (K) of the monochromator* was measured with Cu $K\alpha$ and a Si(333) reflection from a highly perfect crystal; K was 0·989, slightly higher than the value for either an ideally perfect or imperfect monochromator.

* The polarization term is $\frac{1+K\cos^2 2\theta}{1+K}$ where K is $\cos^2 2\theta_{\text{monochromator}}$ for an ideally imperfect crystal.

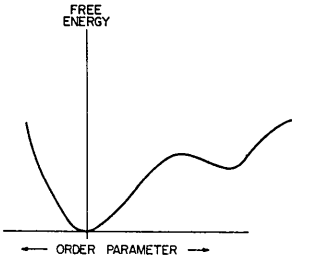

Fig. 1. Free energy *vs* order parameter for a first-order phase change.

The power of the direct beam ($3{\cdot}4\times10^8$ cps) was determined from the integrated intensities of peaks from an aluminum powder compact and from the scattering at high angles from polystyrene. These agreed to within 2·5%.

In the measurement of the direct beam with Al powder, averages of several experimental values of the scattering factor were employed (Batterman, De Marco & Weiss, 1961; De Marco, 1967; Jaarvinen, Merisalo & Inkinen, 1969), with dispersion corrections from the *International Tables for X-ray Crystallography* (1969). A temperature depression $M=0{\cdot}8825\left(\frac{\sin\theta}{\lambda}\right)^2$ was employed and the integrated intensities were corrected for thermal scattering with a minicomputer version of the program developed by Walker & Chipman (1970). For the measurement with polystyrene, the data were corrected for absorption (Milberg, 1958) and double scattering (Warren & Mozzi, 1966; Strong & Kaplow, 1967). The procedure is described by Sparks & Borie (1965), except for the correction for absorption, and that account was taken of the difference in absorption of the coherent and incoherent scattering (2μ for the former, $\mu+\mu'$ for the latter where μ' is the absorption for the modified wavelength). Absorption was calculated from the formulae in the *International Tables for X-ray Crystallography* (1969). The incoherent and coherent scattering per molecule were calculated from the data for C and H (Freeman, 1959; Hanson, Herman, Lea & Skillman, 1964; Keating & Vineyard, 1956; Compton & Allison, 1935). At $\sin\theta/\lambda=0{\cdot}5$, for one molecule of C_8H_8, $I^{\text{coherent}}=22{\cdot}75$ e.u. and $I^{\text{incoherent}}=41{\cdot}91$ e.u.

The crystal was held in a high-temperature, evacuated camera, consisting of a flat Monel base-plate heated with a Nichrome coil and mounted on two orthogonal arcs for alignment. The cover was a hemisphere of beryllium whose absorption was measured as a function of 2θ. The camera itself was mounted on a motorized G.E. quarter circle goniometer. Motion of the crystal and the counter were controlled with a PDP8-L hardware software system (Paavola, Richesson, Morrison & Cohen, 1971); the data were corrected for (measured) dead-time as part of this system.

Temperature was controlled to within $\pm0{\cdot}25$ °C up to 930 °C and $\pm0{\cdot}4$ °C at this temperature with a commercial proportional control system. One chromel–alumel thermocouple was located under the crystal and another was one inch away on the Monel plate. The two gave readings that differed by at most 2 °C. After each temperature change the intensity was monitored until variations subsided. There was a noticeable 'slowing down' of the kinetics near T_c. Alignment was checked at each temperature and adjusted if necessary. The vacuum was 2×10^{-5} torr or better.

The growth of the Cu_3Au single crystal has been described elsewhere (Schwartz & Cohen, 1965). Its composition was within 0·1 at.% of stoichiometry, as determined from the lattice parameter of quenched powder obtained from the crystal. The actual specimen was a trapezoidal slice 1·5 mm thick with a minimum width of 10·4 mm, cut so that the normal to the plate was approximately equidistant from the [001], [101] and [111] directions. It was mechanically and then electrolytically polished, and the effect of surface roughness on the intensity was determined by measuring the angular dependence of the Cu fluorescence excited by Mo $K\alpha$ (de Wolff, 1956; Suortti, 1972).

There are several sources of parasitic scattering that must be corrected for: half-wavelength components, fluorescence from any impurities and Au L fluorescence. The total of these was measured with balanced filters (in the diffracted beam) of Fe and MnO. The resultant contribution was independent of 2θ, and was approximately 6% of a typical data point (which was $\simeq15$ cps) away from a peak in the diffuse scattering. A separate check of scattering due to impurities alone was made by Dr C. J. Sparks on a piece of the same crystal with a solid-state detector and Mo $K\alpha$ radiation. He found no indication of any such scattering. A separate measurement of the amount of half wavelength in the beam with an MgO crystal and the balanced filters indicated that this component was at most 10^{-3} of the Co $K\alpha$. Thus, most of the parasitic scattering was fluorescence.

Air scattering, $\simeq0{\cdot}1$ cps, was measured with a lead beam trap.

Typical counting times were three minutes decreasing to about one minute with increasing temperature; the entire volume in reciprocal space that was measured was completed in five days at the lowest temperature, and two days at the highest.

Data analysis and physical constants

Measurements in a volume in reciprocal space were obtained at 396, 420, 475, 685, 750 and 930 °C. Other data in more limited regions in reciprocal space at other temperatures was also obtained. The lowest temperature was determined to be 2 °C above T_c, by measuring the width of an 001 superstructure reflection with increasing temperature.* This peak increased in breadth discontinuously from 1·3 to 3·7° 2θ at T_c. No change in the breadth of fundamental peaks was detected at this transition.

During the measurements in a volume the monitor count and two points measured early in a run were repeatedly employed as checks by the computer program; measurements were aborted automatically and re-started if these changed by more than a few percent.

The volume to be sampled and the procedures for separating the terms due to local order and displacements have been described by Borie & Sparks (1971) and Gragg & Cohen (1971). The volume was sampled

* The exact temperature may be in error by ±2 °C, as this was the difference in the reading of the two thermocouples.

in reciprocal space at $\simeq 1500$ points in intervals of 0·1 r.l.u. at all but the highest temperature. At this temperature the data was gathered over the same volume at intervals of 0·2 r.l.u. (For subsequent Fourier inversions the intensity at intermediate points was interpolated.)

The total diffuse intensity (I_D) can be written for a binary alloy with one atom per lattice point in terms of the total number of atoms under the beam N, atomic fractions X_A, X_B and scattering factors f_A, f_B, as follows:

$$\begin{aligned} I_D(h_1,h_2,h_3)/N &= I_{SRO}(h_1,h_2,h_3) \\ &+ h_1 Q_x(h_1,h_2,h_3) + h_2 Q_x(h_2,h_3,h_1) + h_3 Q_x(h_3,h_1,h_2) \\ &+ h_1^2 R_x(h_1,h_2,h_3) + h_2^2 R_x(h_2,h_3,h_1) + h_3^2 R_x(h_3,h_1,h_2) \\ &+ h_1 h_2 S_{xy}(h_1,h_2,h_3) + h_2 h_3 S_{xy}(h_2,h_3,h_1) \\ &+ h_3 h_1 S_{xy}(h_3,h_1,h_2) , \end{aligned} \tag{1}$$

where h_i are the coordinates in reciprocal space and N is the number of atoms irradiated.

$$I_D(h_1,h_2,h_3) = \frac{[I_{Total}(h_1,h_2,h_3) - I_{Bragg}(h_1,h_2,h_3)]}{X_A X_B (f_A - f_B)^2} , \tag{2}$$

$$I_{SRO}(h_1,h_2,h_3) = \sum_l \sum_m \sum_n \alpha_{lmn} \cos \pi l h_1 \cos \pi m h_2 \cos \pi n h_3 , \tag{3}$$

$$Q_x(h_1,h_2,h_3) = \sum_l \sum_m \sum_n \gamma^x_{lmn} \sin \pi l h_1 \cos \pi m h_2 \cos \pi n h_3 , \tag{4}$$

$$R_x(h_1,h_2,h_3) = \sum_l \sum_m \sum_n \delta^x_{lmn} \cos \pi l h_1 \cos \pi m h_2 \cos \pi n h_3 , \tag{5}$$

$$S_{xy}(h_1,h_2,h_3) = \sum_l \sum_m \sum_n \varepsilon^{xx}_{lmn} \sin \pi l h_1 \sin \pi m h_2 \cos \pi n h_3 . \tag{6}$$

The 'Fourier coefficients' of the individual diffuse intensity components, Q_x, R_x and S_{xy}, are related to the moments of the displacements in the lattice (static + thermal) by the expressions:

$$\gamma^x_{lmn} = 2\pi [F_{AA} \langle x^{AA}_{lmn} \rangle + F_{AB} \langle x^{AB}_{lmn} \rangle + F_{BB} \langle x^{BB}_{lmn} \rangle] , \tag{7}$$

$$\delta^x_{lmn} = 2\pi^2 [F_{AA} \langle (x^{AA}_{lmn})^2 \rangle + F_{AB} \langle (x^{AB}_{lmn})^2 \rangle + F_{BB} \langle (x^{BB}_{lmn})^2 \rangle] , \tag{8}$$

$$\varepsilon^{xy}_{lmn} = 4\pi^2 [F_{AA} \langle x^{AA}_{lmn} y^{AA}_{lmn} \rangle + F_{AB} \langle x^{AB}_{lmn} y^{AB}_{lmn} \rangle + F_{BB} \langle x^{BB}_{lmn} y^{BB}_{lmn} \rangle] , \tag{9}$$

where,

$$F_{AA} = \frac{f_A^2}{(f_A - f_B)^2} (X_A/X_B + \alpha_{lmn}) , \tag{10}$$

$$F_{AB} = \frac{2 f_A f_B}{(f_A - f_B)^2} (1 - \alpha_{lmn}) , \tag{11}$$

$$F_{BB} = \frac{f_B^2}{(f_A - f_B)^2} (X_B/X_A + \alpha_{lmn}) . \tag{12}$$

The x's are the components of atomic displacements along a [100] direction. The term α_{lmn} is the well-known Warren short-range order parameter,

$$\alpha_{lmn} = 1 - \frac{P^{AB}_{lmn}}{X_B} , \tag{13}$$

where P^{AB}_{lmn} is the conditional probability of finding a B atom at the end of an interatomic vector $la_1/2 + ma_2/2 + na_3/2$, if there is an A at the origin.

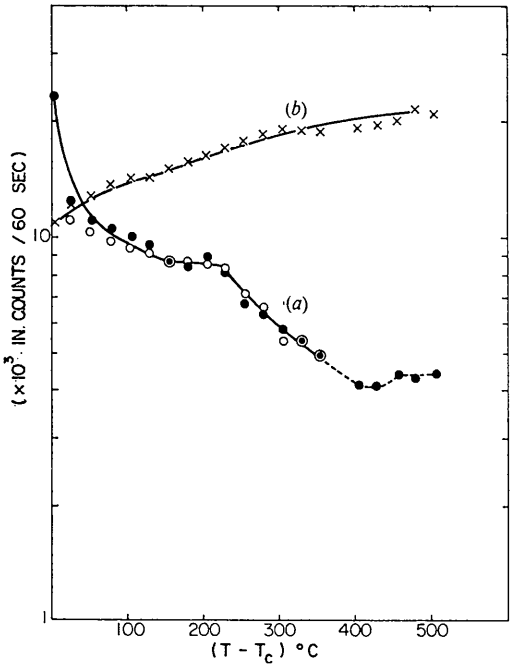

Fig. 2. Intensity at (*a*) 0,0,1 and (*b*) 0,0,1·9 in reciprocal space as a function of the temperature (above the critical temperature, $T_c = 394$ °C.)

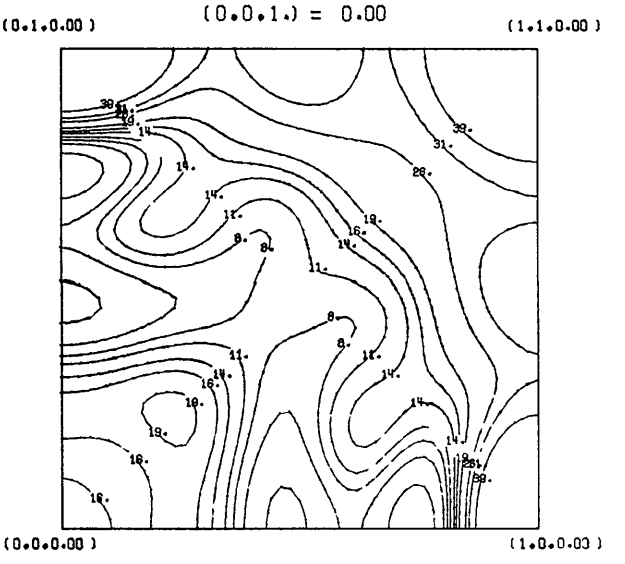

Fig. 3. Short-range order intensity from Cu_3Au at 396 °C; $(h,k,0{\cdot}1)$ section of the reciprocal lattice. Scale: $1 = 1{\cdot}1 \times 10^{-1}$.

The separation procedures yielded I_{SRO}, Q_x, R_x and S_{xy}, in the first octant in reciprocal space, which were then inverted to obtain the Fourier coefficients. At the end of a measurement at one temperature, data was transmitted directly from the minicomputer control to a CDC 6400 computer where all corrections, separations and inversion were carried out. Prior to separation this data was corrected for surface roughness, parasitic and air scattering, nonuniform absorption by the Be hemisphere, placed on an absolute scale and then Compton scattering was subtracted. The scattering factors employed in the program for Cu and Au were averages from the *International Tables for X-ray Crystallography* (1969) and Doyle & Turner (1968), and the dispersion corrections were taken from Cooper (1963). The Compton scattering from Cu was taken from Freeman (1959), and that for Au was estimated from the calculation of James & Brindley (1931) for Hg. A small correction was applied to account for the fact that the K shell of Cu and the K and L shells of Au could not contribute to the Compton process because of the low energy of Co $K\alpha$ radiation.

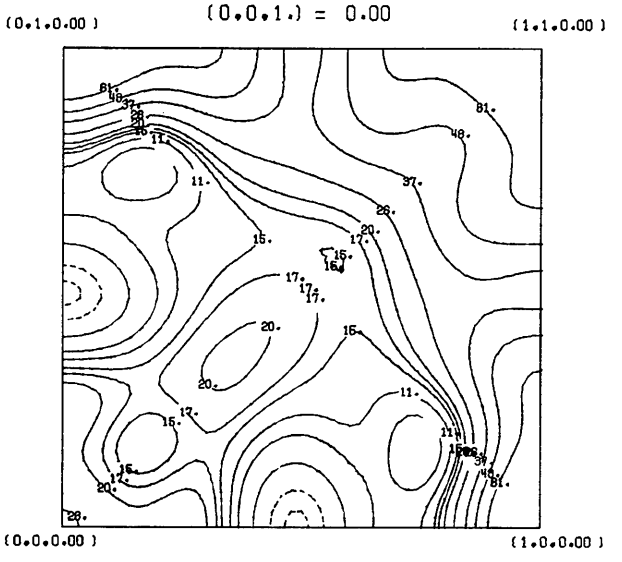

(*a*)

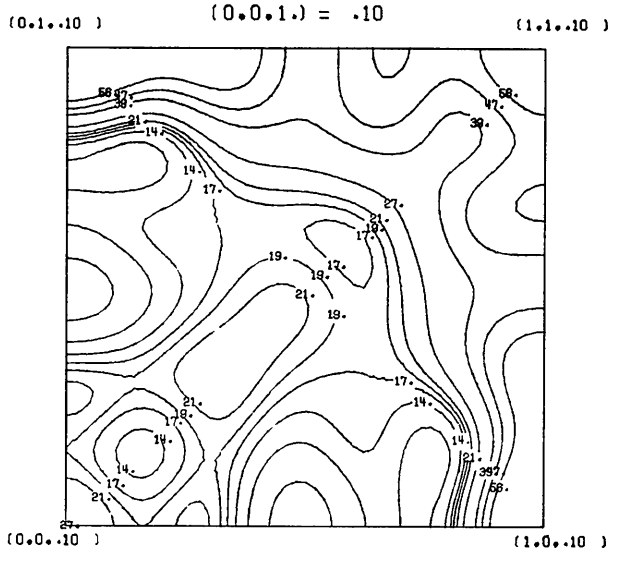

(*b*)

Fig. 4. Short-range order intensity from Cu_3Au at 475 °C; (*a*) $(h,k,0)$ and (*b*) $(h,k,0{\cdot}1)$ sections of the reciprocal lattice. Scales: $1 = 6{\cdot}2 \times 10^{-2}$ and $1 = 5{\cdot}2 \times 10^{-2}$ respectively.

Results

To examine the anomalies in specific heat, the intensity at the 001 position was measured from just above T_c to 925 °C. The results are shown in Fig. 2, where it can be clearly seen that there are discontinuous changes in slope of this intensity near the specific heat anomalies; the changes occur within 50 °C of the reported changes in specific heat. These discontinuities could be due to: (*a*) changes in atomic configurations, (*b*) changes in thermal (or static) atomic displacements, (*c*) changes in alignment of the crystal as the temperature was altered. To ascertain the cause, the intensity at 0,0,1·9 was also measured. The data for this position (in the tail of the 002 fundamental peak) are also given in Fig. 2. It is clear that the changes in slope of the superstructure intensity must be attributed to changes in atomic configurations, not displacements, for there are no such changes at 0,0,1·9, where the diffuse intensity due to displacements is large. However, these 'breaks' were found in only about half the runs attempted.

To clarify the nature of the anomalies, measurements of the diffuse scattering in volumes in reciprocal space were examined. The data to be presented are actually sections in an octant of reciprocal space *synthesized* with short-range order parameters, after the effects of displacements were separated. (The actual parameters are presented and discussed later.) But the same features were detected in the raw data, unless otherwise mentioned; the latter are taken in complex volumes which are less readily visualized with a limited number of sections.

In Fig. 3 contours of this short-range order intensity at 396 °C on the $(h,k,0{\cdot}1)$ plane are given. The disc-shaped intensity profiles are obvious at 100 and 110 positions, which are positions of superlattice peaks for Cu_3Au. These have been detected in all previous studies of this alloy with single crystals (Cowley, 1950*a*, *b*; Moss, 1964). But in addition there is a 50% weaker streak of intensity near $1,\frac{1}{2},0$, a position characteristic of the diffuse scattering from the DO_{22} structure. The intensity about $1,\frac{1}{2},0$ shows the 'cigar-shaped' form characteristic of the local order in a material with a DO_{22} ordered phase. This structure can be simply described as two adjacent unit cells of Cu_3Au with an anti-phase domain on their common {100} plane (Tanner, 1968; Tanner, Clapp & Toth, 1968). The intensity at 100 positions is much greater than that expected at

such points from the intensity at $1,\frac{1}{2},0$ if this intensity at 100 was due to DO_{22} regions. This suggests that both $L1_2$ and DO_{22}-like regions are present in the short-range ordered state. An examination of the other separation components did not reveal a similar contour, so that this effect cannot be attributed to unseparated contributions from size effects.

A similar distribution of intensity was found at 420 °C, although the scattering at $1,\frac{1}{2},0$ was still weaker. The intensity at this position decreased further at 475 °C to $\simeq 25\%$ of that at a 100 position. At 475 °C, there is also an indication of the satellites around 110 positions reported previously in electron diffraction patterns, Fig. 4, but only in separated data. (Note the 'pinching' of intensity at this position.) However along a [100] direction from 110, there are no distinct satellites; the intensity varies smoothly. If this satellite array is in fact due to Kohn-type anomalies associated with flat regions of the Fermi surface, as has been suggested by Moss (1969), there should be a ridge of intensity in a [110] direction near a 110 position, but this was *not* detected. Although the intensity was more diffuse, the cross-like pattern and the intensity at $1,\frac{1}{2},0$ was also detected at 685 °C, just above the first transition. At 750 and 930 °C the cross had disappeared and the intensity at $1,\frac{1}{2},0$ did not exhibit the broad cigar-shaped profile of the DO_{22} type structure. A new striking feature of the intensity at 930 °C was the peaking at $\frac{1}{2},\frac{1}{2},\frac{1}{2}$ shown in Fig. 5. Closer examination of the data revealed that a very weak, broad local-order intensity was present at this position at all lower temperatures. Such an intensity has been recently detected in quenched, disordered Cu_3Pt by electron diffraction by Ohshima & Watanabe (1973), but has not been reported before for Cu_3Au. This region of scattering could be due to local CuPt-like regions or $CuPt_3$-like regions (Clapp & Moss, 1968), that is, fluctuations with alternating Cu and Au-rich (111) planes.

It appears then that the first anomaly is associated with the disappearance of small local fluctuations resembling DO_{22}-like arrays, whereas at the higher temperature there is the formation of small layered arrays. We shall return to this point later, when considering computer simulations of the atomic configurations.

For the quantitative analysis it was necessary to include a correction factor to the scattering factors for temperature. This was approximated by the form $(f_A - f_B)^2 \exp(-2B \sin^2\theta/\lambda^2)$. The term B was evaluated by comparing the intensities at 300 and 100 positions, after correcting the data for surface roughness, parasitic scattering, Compton and thermal diffuse scattering, the last being calculated following Walker & Chipman (1970). [At 405 and 450 °C Moss (1964) reported that the intensity ratio I_{300}/I_{100} (corrected for Δf^2 and the polarization factor) was 0·92. In our work this ratio at 420 °C was 0·87.]

The values of B determined in this way are shown in Fig. 6. The large increase near T_c is indeed surprising. The B values were determined in a somewhat crude manner (there appears, though, to be no other way). However, support that a real effect was observed is presented in Fig. 7. This figure shows the variation with temperature of the leading coefficient in equation (5). This coefficient,* δ_{000}, represents the total intensity

* Formally, δ_{000} should have a null value, but a large negative portion immediately under the Bragg peak is inaccessable to measurement.

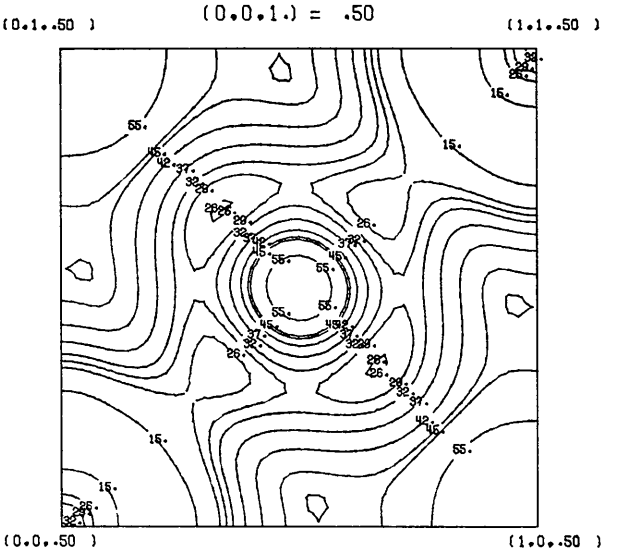

Fig. 5. Short-range order intensity from Cu_3Au at 930°; $(h,k,0{\cdot}5)$ section of the reciprocal lattice. Scale: $1 = 1{\cdot}9 \times 10^{-2}$.

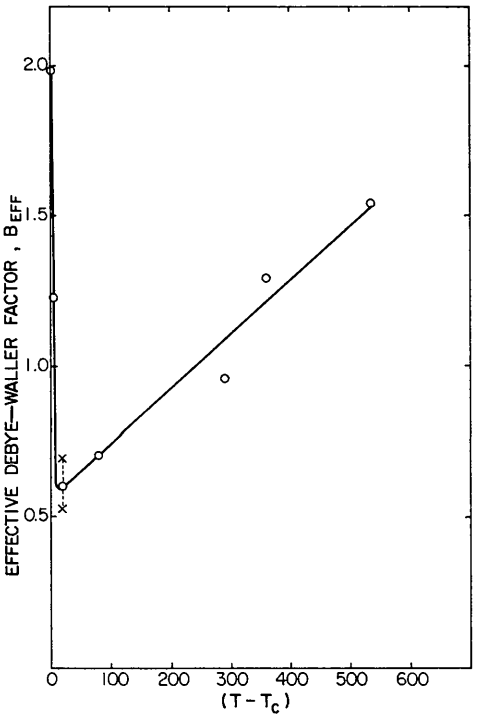

Fig. 6. Effective Debye–Waller Factor *vs* T for Cu_3Au measured from the 001 and 003 intensities in reciprocal space.

away from Bragg peaks due to mean-square static and dynamic displacements. The increased peak depression is matched by a sharp rise in this displacement intensity. There are a few results in the literature concerning measurements at temperature of the Debye–Waller factor of Cu_3Au from fundamental peaks, which indicate a rise of $\simeq 30\%$ just below T_c (Owen & Evans, 1967; Towers, 1972; Tibballs, 1974), but this is the first indication of a premonitory effect just *above* T_c in Cu_3Au. It is not certain whether this increase is due to a rise in static or dynamic distortions, but as discussed in the introduction, if the free-energy curve has one or more subsidiary minima above T_c it is likely that these are quasi-static effects. Further work with neutron scattering techniques is now underway to eliminate this ambiguity.

The diffuse intensity obtained in a volume in reciprocal space in this study was separated into its components due to local order and displacements, restored in the first positive octant in reciprocal space by symmetry considerations for each term, and then extrapolated through Bragg peaks with a polynomial fit from surrounding points, generally from $\Delta h = 0{\cdot}2$ away from a Bragg peak; in this way subjective considerations of the data were avoided. The symmetry of the intensity components was examined; any difference at symmetry-related points was within the estimated statistical counting error of $\pm 15\%$. (A typical data point was 3200 counts, but in the symmetry separation some five of these points are involved.)

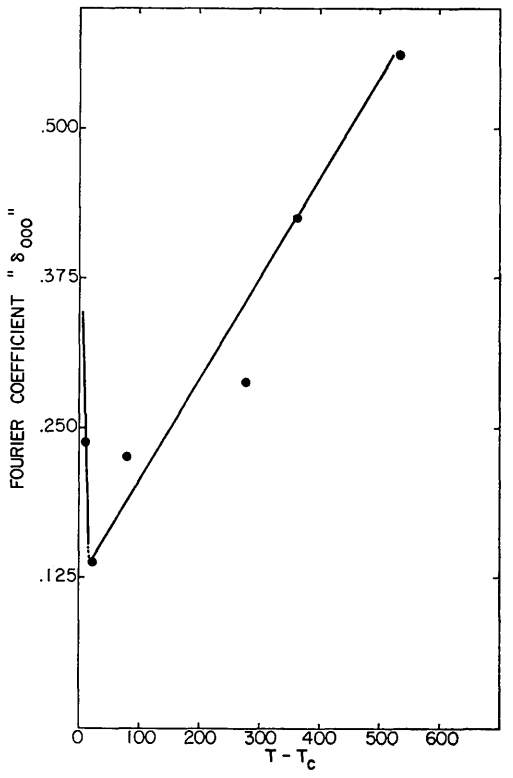

Fig. 7. The effect of temperature on δ_{000}, the net second-order displacement scattering, in Cu_3Au.

The evaluation of errors in the separation of the data with the technique employed here have been discussed by Gragg, Hayakawa & Cohen (1973) and Hayakawa, Bardhan & Cohen (1975). In both the separation and inversion, it is assumed that in the displacement terms the scattering factor ratios,

$$\left(\frac{f_{Cu}}{f_{Au}-f_{Cu}}\right) \text{ and } \left(\frac{f_{Au}}{f_{Au}-f_{Cu}}\right),$$

are constant [see equations (4)–(12)]. Actually, however, these vary by 20–25% across the volume of measurement. Therefore, after the analysis at 420 and 750°C, data were synthesized with the Fourier coefficients, and varying scattering factor; Compton scattering, background, *etc.* were added, as well as statistical error. Then this synthesized intensity was reanalyzed assuming constant scattering factor ratios. The errors in α and γ at 420°C were estimated to be of the order of 5% (absolute errors of 10^{-2}) except for $\alpha(211)$ and $\alpha(220)$ which were in error by 15 and 24% respectively. At 750°C, where thermal diffuse scattering, TDS, is higher, the absolute error in the α's was $\simeq 10^{-3}$, leading to an error of $\simeq 20\%$ in α_{110}, 100% in $\alpha(211)$, $\alpha(220)$ and $\alpha(310)$, and 20% for all γ's.

It might be thought that calculating TDS and subtracting it would reduce errors by reducing the magnitude of the displacement terms. This was attempted with data at 685°C using the elastic constants determined by Siegel (1940). The effect was to cause $\simeq 9\%$ of the data for R_x to be negative, despite the fact that only the intensity due to dynamic displacements was being subtracted, not that due to static displacements which is also part of R_x. This procedure is therefore not satisfactory. The effect on the α's was $\simeq \pm 0{\cdot}03$ for $\alpha(110)$ but much less for higher terms; α_{000} was increased by $\simeq 10\%$.

As has been mentioned earlier, the temperature correction applied in this study is only an approximation; the temperature factor should vary with the value of *lmn* (Walker & Keating, 1963; Hayakawa *et al.*, 1975). However, calculation showed that the changes in intensity with such a variation were much less than the statistical error.

Finally Gragg *et al.* (1973) have shown how to estimate higher-order terms in the effects due to static and dynamic displacements than those included in equation (1). These calculations for data at 750°C indicated that the error in $\alpha(110)$ was less than 1%, but was 25–75% for $lmn = 200$–222, after which it again became small.

Some of these errors tend to cancel, so that by way of summary, it is estimated that the error for $\alpha(110)$ is $\pm 25\%$, $\simeq \pm 15\%$ for $\alpha(200)$, $\alpha(211)$ and $\alpha(220)$, and $\simeq \pm 10\%$ for higher α's.

The Fourier coefficients for all six temperatures at

which measurements in a volume were made are given in Tables 1–6. The values of the α's are considerably lower than those in the earlier, less complete studies (Cowley, 1950; Moss, 1964). There is surprisingly good agreement with a re-analysis by Walker & Keating (1963) of Cowley's data, in which some approximate corrections for scattering due to displacements were applied.

The value of $\alpha(000)$ in Tables 1–6 should, by definition, be unity as $\alpha(000) \equiv 1 - P^{AB}(000)/X_B = 1 - 0/X_B$.

Table 1. *Experimentally determined Fourier coefficients* ($\times 10^3$) *of the diffuse intensity components in* Cu_3Au *at* 396°C

lmn	α_{lmn}	γ^X_{lmn}	γ^Y_{lmn}	γ^Z_{lmn}	δ^X_{lmn}	δ^Y_{lmn}	δ^Z_{lmn}	ε^{XY}_{lmn}	ε^{YZ}_{lmn}	ε^{ZX}_{lmn}
000	1641	0	0	0	237	237	237	0	0	0
110	−103	−27	−27	0	39	39	57	29	0	0
200	246	−212	0	0	27	37	37	0	0	0
211	42	−106	−30	−30	11	24	24	7	−9	7
220	77	−76	−76	0	27	27	20	34	0	0
310	−100	77	−2	0	1	20	16	22	0	0
222	33	−48	−48	−48	19	19	19	14	14	14
321	−5	−70	−43	−78	3	13	8	13	−1	−1
400	78	−119	0	0	2	18	18	0	0	0
411	3	−135	−5	−5	3	11	11	10	−1	−10
330	−16	−58	−58	0	8	8	9	13	0	0
420	46	−102	−37	0	10	14	19	35	0	0
332	−15	−49	−49	−44	6	6	7	11	6	6
422	39	−93	−37	−37	4	9	9	18	−3	18
431	−11	−81	−39	−5	5	4	6	26	−4	3
510	−59	−100	4	0	−4	16	11	12	0	0
521	−20	−80	−12	2	−7	8	8	19	−10	1
440	6	−47	−47	0	5	5	2	41	0	0
530	−25	−60	−5	0	−2	5	2	18	0	0
433	−9	−64	−33	−33	2	2	2	13	−2	13
600	31	−82	0	0	5	2	2	0	0	0
442	27	−52	−52	−25	3	3	2	25	3	3
611	23	−85	4	4	−5	2	2	4	−2	4
532	−16	−57	−21	−20	−3	6	4	16	7	11
620	29	−65	−12	0	3	5	0	17	0	0
622	19	−70	−12	−1	1	5	5	13	−7	13
631	7	−69	−11	−6	−2	1	−2	18	−4	5

Table 2. *Experimentally determined Fourier coefficients* ($\times 10^3$) *of the diffuse intensity components in* Cu_3Au *at* 420°C

lma	α_{lmn}	γ^X_{lmn}	γ^Y_{lmn}	γ^Z_{lmn}	δ^X_{lmn}	δ^Y_{lmn}	δ^Z_{lmn}	ε^{XY}_{lmn}	ε^{YZ}_{lmn}	ε^{ZX}_{lmn}
000	1107	0	0	0	139	139	139	0	0	0
110	−93	25	25	0	4	4	26	7	0	0
200	141	−128	0	0	14	8	8	0	0	0
211	35	−35	−9	−9	−0	7	7	−7	1	−7
220	50	−36	−36	0	9	9	−1	19	0	0
310	−99	9	17	0	1	1	9	3	0	0
222	18	−6	−6	−6	5	5	5	3	3	3
321	−6	−13	−4	4	−1	2	−0	−4	−7	−2
400	75	−36	0	0	2	3	3	0	0	0
411	17	−30	−5	−5	−2	5	5	0	3	0
330	−19	3	2	0	5	5	4	−10	0	0
420	38	−22	−17	0	1	5	0	11	0	0
332	1	−4	−4	−10	−1	−1	−0	−5	−3	−5
422	20	−16	−8	8	2	1	1	−0	0	−0
431	−2	−13	−14	3	0	1	1	−2	−1	−4
510	−31	−7	6	0	1	1	1	2	0	0
521	3	8	−1	4	−5	1	−1	0	−3	−0
440	10	−10	−10	0	2	2	−0	2	0	0
530	−9	4	4	0	2	2	1	−3	0	0
433	4	−15	−4	−4	−2	−1	−1	−2	−1	−2
600	25	−20	0	0	−1	0	0	0	0	0
442	8	−9	−9	2	1	1	0	−1	−0	−1
611	16	−11	−1	−1	−2	−0	−1	−2	2	−2
532	−3	−3	−3	−1	−1	1	0	−2	−2	−3
620	6	−7	−15	0	1	1	−0	7	0	0
622	11	−7	−4	−4	−2	−1	−1	−0	0	−0
631	0	−4	−8	0	1	−0	−1	−2	1	−4

There is clearly some unaccounted-for intensity in I_{SRO}. It appears that this is due to incomplete separation of the intensity due to displacements, because the value is largest at 396°C where this intensity is large and after decreasing at 420°C, again increases with temperature. Cowley renormalized his data by dividing by $\alpha(000)$, but this has been avoided here; if the extra intensity is fairly constant in reciprocal space, the $\alpha(lmn)$ other than $\alpha(000)$ are not affected.

The absolute values of α and γ are plotted in Fig.

Table 3. *Experimentally determined Fourier coefficients* ($\times 10^3$) *of the diffuse intensity components in* Cu_3Au *at* 475°C

lmn	α_{lmn}	γ^X_{lmn}	γ^Y_{lmn}	γ^Z_{lmn}	δ^X_{lmn}	δ^Y_{lmn}	δ^Z_{lmn}	ε^{XY}_{lmn}	ε^{YZ}_{lmn}	ε^{ZX}_{lmn}
000	1239	0	0	0	228	228	228	0	0	0
110	−107	53	53	0	11	11	17	−17	0	0
200	138	−111	0	0	−2	6	6	0	0	0
211	45	−41	−4	−4	−4	2	2	−7	−4	−7
220	45	−37	−37	0	2	2	−10	9	0	0
310	−86	−9	23	0	−5	−1	−0	−3	0	0
222	15	−10	−10	−10	−2	−3	−2	3	3	3
321	3	−23	−10	4	−5	−0	−5	2	−6	−3
400	52	−26	0	0	−3	−2	−2	0	0	0
411	20	−46	−20	−20	−10	−1	−1	0	2	0
330	−18	−7	−7	0	−0	−0	−5	−13	0	0
420	19	−28	−15	0	−7	2	−3	−13	0	0
332	4	−16	−15	−3	−4	−4	−3	−6	4	−6
422	10	−27	−8	−8	−4	−2	−2	3	1	3
431	−3	−22	−16	7	−4	−1	−4	6	−1	−5
510	−25	−23	9	0	−4	1	−2	−7	0	0
521	−13	−18	3	6	−7	−1	−2	8	−5	−1
440	−1	−22	−21	0	1	2	−4	7	0	0
530	2	−0	1	0	−3	−1	−4	−10	0	0
433	0	−17	−6	−6	−4	−2	−2	−0	2	−0
600	41	−9	0	0	−5	−3	−3	0	0	0
442	1	−13	−13	1	−3	−3	−2	5	−0	5
611	7	−10	−4	−4	−3	0	0	−1	4	−1
532	−5	−10	−3	5	−5	−0	−1	−1	−3	−1
620	27	−4	−9	0	−4	−2	−6	6	0	0
622	24	−7	1	1	−7	−4	−4	−0	−2	−0
631	−4	−5	−14	1	−2	−1	−2	0	0	−3

Table 4. *Experimentally determined Fourier coefficients* ($\times 10^3$) *of the diffuse intensity components in* Cu_3Au *at* 685°C

lmn	α_{lmn}	γ^X_{lmn}	γ^Y_{lmn}	γ^Z_{lmn}	δ^X_{lmn}	δ^Y_{lmn}	δ^Z_{lmn}	ε^{XY}_{lmn}	ε^{YZ}_{lmn}	ε^{ZX}_{lmn}
000	1369	0	0	0	288	288	288	0	0	0
110	−68	49	49	0	9	9	22	−21	0	0
200	118	−110	0	0	−8	−4	−4	0	0	0
211	54	−44	−15	−15	−11	−0	−0	−12	−8	−12
220	26	−42	42	0	−1	−1	−8	2	0	0
310	−82	−13	11	0	−9	−0	−1	3	0	0
222	−2	−20	−20	−20	−4	−4	−4	1	1	0
321	1	−33	−10	−2	−7	−1	−5	1	−8	2
400	35	−29	0	0	−12	1	1	0	0	0
411	−0	−45	−79	−79	−9	−0	−0	−1	3	−1
330	−1	−15	−15	0	−2	−2	−0	−2	0	0
420	3	−41	−22	0	−7	−2	−4	−7	0	0
332	3	−21	−21	−13	−5	−5	−4	2	−2	−2
422	2	−31	−10	−10	−5	−3	−3	−4	0	4
431	−1	−24	−19	−0	−6	−2	−1	3	0	−4
510	−18	−32	−3	0	−2	4	1	5	0	0
521	−4	−28	−7	−5	−5	0	−1	5	−3	1
440	−16	−21	−21	0	0	0	−1	8	0	0
530	−5	−16	−19	0	−2	2	−1	5	0	0
433	7	−27	−16	−16	−4	−2	−2	3	3	1
600	10	−31	0	0	3	0	0	0	0	0
442	2	−21	−21	−6	−2	−2	−1	4	−0	−0
611	6	−22	−3	−3	−4	2	2	1	3	1
532	−4	−22	−10	−9	−3	−0	1	4	1	1
620	−1	−20	−15	0	−2	4	1	9	0	0
622	7	−19	−6	−6	−2	0	0	3	−1	3
631	−2	−17	−9	−1	0	−0	1	3	−1	−1

8(*a*) and (*b*). There are a number of interesting features of these Fourier coefficients.

(*a*) As has been reported earlier (Warren, Averbach & Roberts, 1951; Moss, 1964), the intensity modulation term involving γ [equation (4)] oscillates, being negative for Cu_3Au below the 100 position, positive between 100 and 200, *etc.* However, the difference between the intensity below and above 100 is much smaller at 396 °C than at higher temperatures. This is due to the fact that $\gamma(110)$ is negative at 396 °C, but

Table 5. *Experimentally determined Fourier coefficients* ($\times 10^3$) *of the diffuse intensity components in* Cu_3Au *at* 750 °C

lmn	α_{lmn}	γ^X_{lmn}	γ^Y_{lmn}	γ^Z_{lmn}	δ^X_{lmn}	δ^Y_{lmn}	δ^Z_{lmn}	ε^{XY}_{lmn}	ε^{YZ}_{lmn}	ε^{ZX}_{lmn}
000	1442	0	0	0	428	428	428	0	0	0
110	−76	47	47	0	35	35	26	−27	0	0
200	70	−49	0	0	10	24	24	0	0	0
211	7	6	5	5	8	15	8	−13	−22	−13
220	−1	4	4	0	10	10	7	−26	0	0
310	−41	17	5	0	2	9	9	−2	0	0
222	4	4	4	4	9	9	9	−13	−13	−13
321	−11	2	4	2	5	8	6	−16	−9	−4
400	24	−8	0	0	−10	−3	−3	0	0	0
411	10	−6	−1	−1	−2	−5	−5	−4	1	−4
330	−11	−1	−1	0	6	6	6	−14	−14	0
420	32	−9	−1	0	4	10	7	−4	0	0
332	−1	−5	−5	−2	2	2	4	−9	−9	−9
422	−2	−5	−4	−4	−2	0	0	−7	−3	−7
431	−4	−5	−5	2	2	4	4	−7	−6	−5
510	−0	−9	−3	0	−1	2	1	4	0	0
521	1	−7	−1	2	−2	3	2	−3	−1	−5
440	−19	−4	−4	0	2	2	2	−7	−7	0
530	−3	−4	−4	0	0	3	4	−2	0	0
433	−6	−5	−3	−3	1	2	2	−4	−1	−4
600	12	−18	0	0	1	3	3	0	0	0
442	0	−7	−7	−2	3	3	4	−6	−2	−2
611	11	−10	−0	−0	−3	1	2	−0	−6	−0
532	2	−8	−5	−2	−1	3	2	−1	−2	−2
620	3	−6	−2	0	−7	−0	−1	0	−0	0
622	4	−13	−1	−1	0	3	3	0	1	0
631	7	−12	−2	−1	−3	1	1	−1	2	1

Table 6. *Experimentally determined Fourier coefficients* ($\times 10^3$) *of the diffuse intensity components in* Cu_3Au *at* 930 °C

lmn	α_{lmn}	γ^X_{lmn}	γ^Y_{lmn}	γ^Z_{lmn}	δ^X_{lmn}	δ^Y_{lmn}	δ^Z_{lmn}	ε^{XY}_{lmn}	ε^{YZ}_{lmn}	ε^{ZX}_{lmn}
000	898	0	0	0	568	568	568	0	0	0
110	33	62	62	0	40	40	362	−28	0	0
200	137	−39	0	0	26	10	10	0	0	0
211	85	16	22	22	5	11	11	−11	−21	−12
220	60	16	16	0	8	8	−14	−21	0	0
310	−1	11	25	0	9	5	−0	−1	0	0
222	42	17	17	17	−8	−8	−8	−12	−12	−12
321	18	−2	18	−20	1	1	1	−15	−11	−48
400	53	−16	0	0	17	8	8	0	0	0
411	10	−14	17	17	−0	2	2	−45	1	−45
330	14	−4	−4	0	3	3	−7	−13	0	0
420	13	−17	13	0	1	10	−0	−4	0	0
332	10	−10	10	9	−5	−5	−7	−9	−10	−10
422	10	−15	82	82	−2	−3	−3	−7	−5	−7
431	5	−14	94	18	−4	4	−1	−6	−78	−5
510	0	0	14	0	8	12	8	4	0	0
521	−2	1	12	18	−4	7	1	−4	−2	−6
440	16	−14	−14	0	5	5	−2	−6	0	0
530	6	4	−9	0	0	10	0	−3	0	0
433	4	−17	−11	−10	−9	−1	−1	−6	−2	−6
600	18	11	0	0	19	1	1	0	0	0
442	4	−18	−18	8	−2	−2	4	−6	−3	−3
611	4	17	17	17	2	5	5	−0	−1	−1
532	−0	−1	−11	7	−10	2	2	−3	−4	−3
620	15	20	10	0	−2	2	−5	−0	0	0
622	−2	13	9	9	−9	−0	−0	−2	−3	−2
631	1	12	−9	13	−5	4	1	−4	2	−3

positive above this temperature, which implies [see equation (4)], that the dominant term in γ, the interatomic displacement $\langle X_{110}^{Cu-Cu} \rangle$ is positive at the lowest temperature, whereas it is negative at higher temperatures; only this latter value would be expected from the sizes of Au and Cu atoms. The investigation with neutron scattering now under way may clarify this unusual feature. Recall that it is close to T_c where the mean-square size effect terms and the temperature depression of the peaks also increase drastically.

(*b*) The magnitude of $\gamma(110)$ increases with temperature. At 750°C $|\gamma(110)| \simeq |\gamma(200)|$ and at 930°C $|\gamma(110)| \simeq 2|\gamma(200)|$.

(*c*) There is a periodicity of 7–8 neighbors in the

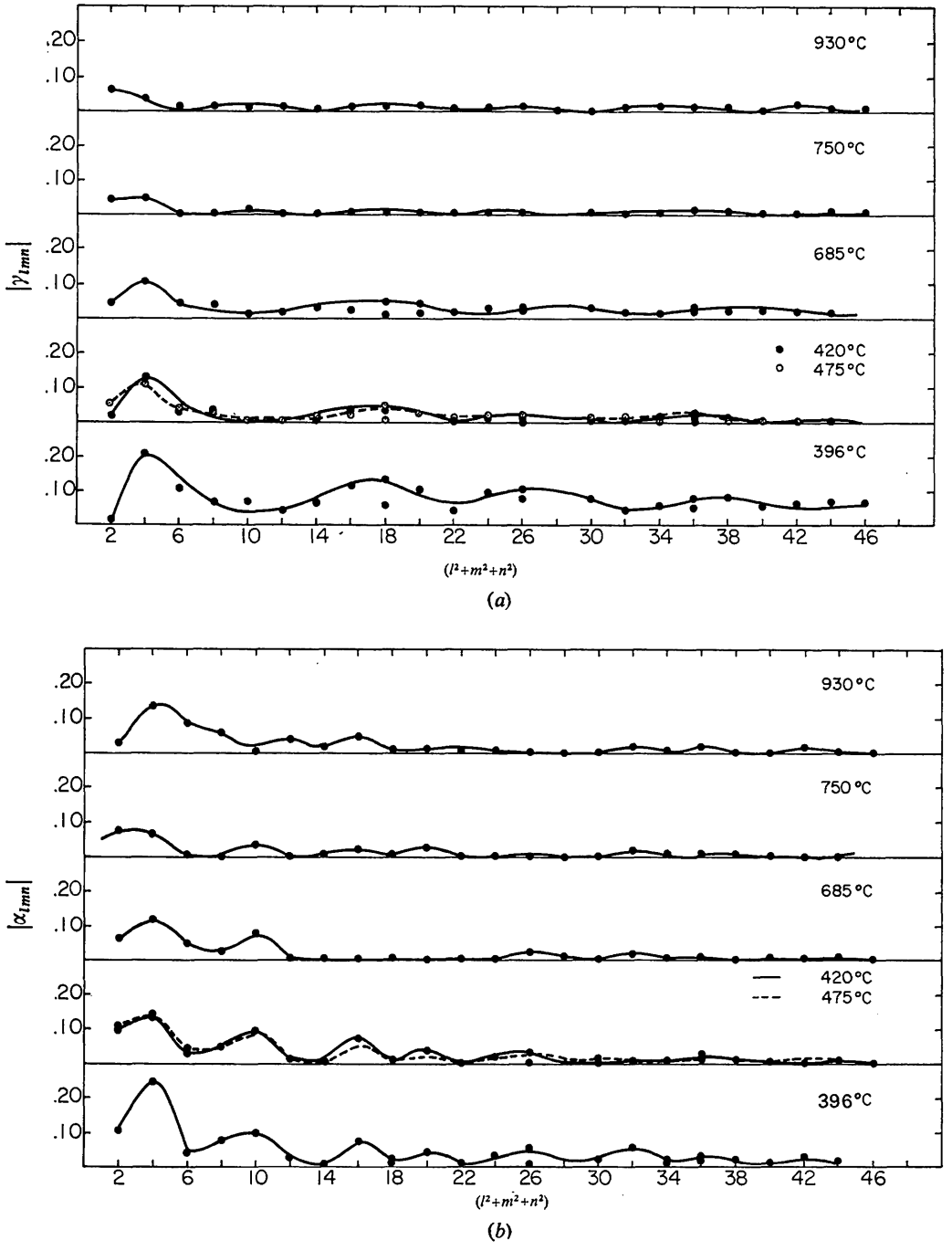

Fig. 8. (*a*) The variation of the size-effect Fourier coefficient $|\gamma_{lmn}|$ as a function of $(l^2+m^2+n^2)$ at different temperatures. (*b*) The variation of the short-range order coefficient $|\alpha_{lmn}|$ as a function of $(l^2+m^2+n^2)$ at different temperatures.

oscillations in γ, decreasing somewhat at the two highest temperatures. This oscillation is *not* the same as the oscillations in the α's; compare Fig. 8(*a*) and (*b*).

(*d*) The large values of $\gamma(200)$ and $\gamma(420)$ and the low value of $\gamma(130)$ suggest that any ordered regions contain antiphase domains on {100} type planes, with the shift to cause the boundary within the plane. Such planes would lead to wrong bonds in a ⟨100⟩ direction but not in the plane itself. This supports the suggestion from the intensity itself that there are DO_{22}-like regions in the short-range ordered state.

As for the term involving averages of quadratic terms in displacements [R_x,S_{xy}, equations (5), (6), (8), (9)] it has already been mentioned that there was a dramatic increase in this intensity near T_c but that otherwise there was just a steady increase with temperature as would be expected due to first-order TDS alone. The usual peaking of these terms under Bragg peaks was observed.

Discussion

The unusual changes in short-range order intensity at 600 and 850°C appear to be associated with distinct changes in the atomic configurations associated with the short-range order. The marked change in sign of γ, the first Fourier coefficient of the intensity due to the mean atomic displacements (δ_{000}), and the rapid rise in mean square displacements close to T_c are also remarkable, but further comment must await studies by neutron inelastic scattering.

The development of a one-dimensional periodic antiphase domain structure during the initial stages of ordering in Cu_3Au only at low temperatures reported by Guinier & Griffoul (1948) can now be understood. De Fontaine (1976) has pointed out that, as in spinodal decomposition, spinodal ordering can occur. That is, on quenching below a spinodal for ordering, composition fluctuations will develop for those amplitudes which have favorable amplification factors. Those waves that are initially amplified will be those with wave vectors where the diffuse intensity above the spinodal is peaked. One such vector found in this study is $[1,\frac{1}{2},0]$ which appears to be due to DO_{22}-like regions. As this structure is two antiphased $L1_2$ cells, the nuclei of a long-period superlattice are already present above T_c.

Since the original work by Gehlen & Cohen (1965) it has been found useful to obtain information on the chemical make-up of the local atomic arrays by rearranging several thousand atoms in a computer model until agreement is obtained with several of the measured short-range order parameters.

This technique has been reviewed recently (Gragg, Bardhan & Cohen, 1971). Monte Carlo calculations involving 4000 atoms and first and second-neighbor energies by Golosov & Dudka (1973) have substantiated the results of such simulations. In addition, direct comparisons have been made to field-ion images (Berg, Tsong & Cohen, 1973), and many of the details, such as the size of ordered regions and the presence of domain boundaries within them, have been confirmed by lattice imaging in the electron microscope by Sinclair & Thomas (1975). Modelling in this manner was performed in this study with 4000 atoms; the first six $\alpha(lmn)$ were satisfied to 0·5%. Several other α's calculated from the resultant configurations are presented in Table 7 and may be compared to the actual values in Tables 1–6.

Fig. 9(*b*)–(*e*) gives the distribution of Au atoms around a given Au atom in the first three shells; Fig. 9(*a*) gives these distributions for a random alloy. Only at the highest temperature does the system appear nearly random. But in fact it is *not* random. The total number of near-neighbor Au–Au first-neighbor pairs can be written in terms of triplets:

$$N^{\mathrm{AuAu}}(110)=N^{\mathrm{AuAuAu}}(110)+N^{\mathrm{AuAuCu}}(110)\ . \quad (14)$$

This value and the total number of Au–Au–Au and Cu–Cu–Cu triplets are plotted *vs* temperature in Fig. 10. At the highest temperature there is a tendency for *clustering* of Au atoms. That this might occur was first speculated by Kuczynski *et al.* (1956). Consider next the second-neighbors around an Au atom. For fully ordered Cu_3Au, there are 6 Au atoms in this position and 1·5 for a random alloy. The number of Au atoms with no Au atoms in the second shell is given in Table 8. There is a considerable tendency for ordering in this second shell at 930°C.

Table 8. *Number of* Au *atoms with no* Au *atoms as second neighbors*

Random	396°C	420°C	475°C	685°C	750°C	930°C
184	32	88	92	97	113	78

Table 7. *Results of computer simulations for* Cu_3Au

α_{lmn} satisfied up to α_{222}, other α_{lmn}'s calculated. Starting configuration was always a near-random alloy.

lmn	$\sigma(\alpha_{lmn})$*	396°C	420°C	475°C	685°C	750°C	930°C
α_{321}	0·0013	−0·0113	−0·0076	−0·0046	0·0039	0·0051	0·0217
α_{400}	0·0037	0·0951	0·0911	0·1044	0·0671	0·0440	0·0453
α_{330}	0·0026	−0·0209	0·0078	0·0040	0·0118	0·0000	0·0193
α_{420}	0·0019	0·0269	0·0313	0·0407	0·0131	0·0029	0·0230
No. of Jumps		829	695	868	710	418	842

* $\sigma(\alpha_{lmn})=(X_B/NZ_{lmn}X_A)^{1/2}$ is the expected standard deviation of the short-range order parameter, α_{lmn} as given by Williams (1970); X_B and X_A are the solute and solvent concentrations respectively, N is the size of the lattice used in the simulation (in the present case, $N=4000$ atoms) and Z_{lmn} is the coordination number of shell *lmn*.

Finally, the various triplet and quadruplet probabilities are given in Table 9, along with the theoretical values of Golosov, Popov & Pudan (1973) employing the Kikuchi cluster variation method. It is seen from this table that the present measurements show a greater degree of disorder than that predicted. Since all approximate theories yield a T_c greater than the observed T_c (Guttman, 1955) this discrepancy is not unexpected.

The actual computer simulations were examined on several planes. Up to 475 °C, there is little change in the total volume of ordered regions, although there is a small reduction in size. At 750 °C there is a reduction of $\simeq 66\%$ in the volume of ordered material.

At 396 °C only 4% of the Au atoms are not in ordered surroundings (defined as 0, 1, or 2 Au atoms in the first shell and 3, 4, 5 or 6 Au atoms in the second shell, whereas for Cu atoms the corresponding quantities were taken as 4 and 0 or 1). There are almost continuous Cu_3Au-like ordered regions piercing the model, with ordered regions $\simeq 4 \times 3 \times 3$ cells in size, antiphase

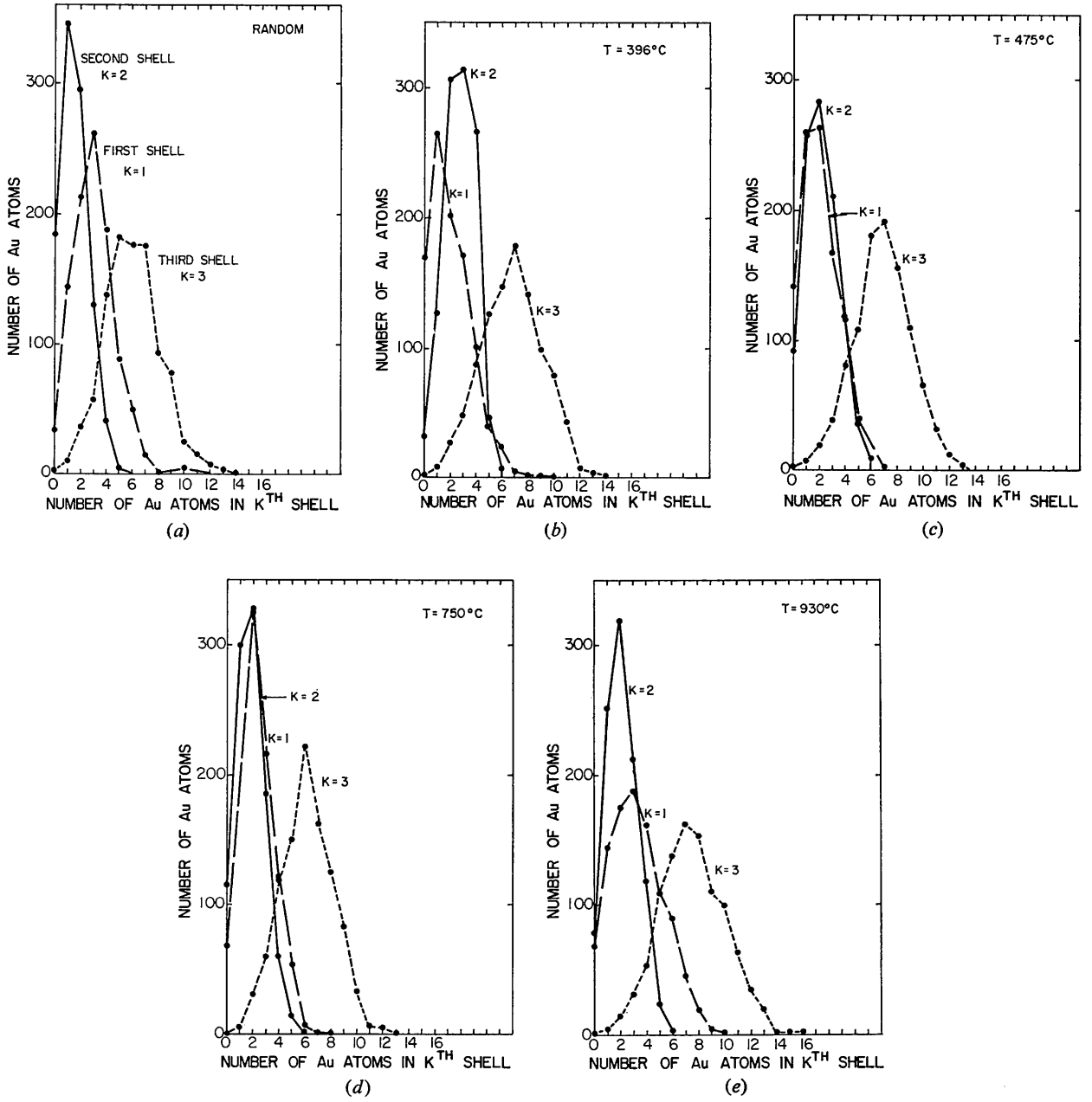

Fig. 9. (*a*) Distribution of Au atoms around an Au atom in the *k*th shell for $k = 1, 2$ and 3, in Cu_3Au. (*a*) $\alpha_1 = \alpha_2 = \alpha_3 = 0{\cdot}0$, a near random alloy. (*b*) 396 °C ($\alpha_1 = -0{\cdot}103$ $\alpha_2 = 0{\cdot}246$, $\alpha_3 = 0{\cdot}042$). (*c*) 475 °C ($\alpha_1 = 0{\cdot}107$, $\alpha_2 = 0{\cdot}138$, $\alpha_3 = 0{\cdot}045$). (*d*) 750 °C ($\alpha_1 = -0{\cdot}076$, $\alpha_2 = 0{\cdot}070$, $\alpha_3 = 0{\cdot}007$). (*e*) 930 °C ($\alpha_1 = 0{\cdot}003$, $\alpha_2 = 0{\cdot}137$, $\alpha_3 = 0{\cdot}085$).

with respect to each other. In addition there are $\simeq 4\times10^{20}$/cc DO_{22} cells. The DO_{22} cells appeared to be stacked. At 475 °C the situation is similar except that the density of DO_{22} cells is about one third the value at 396 °C. Small CuAu-like regions (6×10^{19}/cc were found, the largest containing eight atoms. Such regions could be found with some difficulty at 396 °C, but were rarely thicker than 1–2 planes. At 750 °C the density of Cu_3Au regions is quite large ($\simeq 8\times10^{20}$/cc) and involve 18–25 atoms, at least two layers thick. These regions are remarkably well separated by at least three disordered matrix cells. The density of CuAu-like regions was $\simeq 6\times10^{20}$/cc, with an average size of nine atoms and involving 40 % of the Au atoms. These were generally at the boundaries of Cu_3Au-like regions. Only nine of the 1000 Au atoms were isolated.

At 930 °C, there are (100) platelets of CuAu-like regions, as long as four unit cells in one direction, 2–3 atomic layers thick with a density of 3×10^{20}/cc. At the ends of such platelets there are {111} layer-like regions, 10–12 atoms in size, 3–4 layers thick containing 80 % or more of Au, or Cu, as in the CuPt-like structure. There are also some regions of Cu_3Au.

Interatomic potentials can be determined from the short-range order parameters, as was first shown by Cowley (1950*b*). Since that time a number of workers have investigated this point: Clapp & Moss (1966, 1968), Wilkins (1970), Tahir-Kheli (1969), Taggart & Tahir-Kheli (1973), Shirley (1974), and Ashcroft (1972). The particular interest in these studies was to show that there was indeed an oscillatory potential due to incompletely screened ion cores, as was first predicted theoretically by Friedel (1954), and also to investigate any variation of this potential with temperature. In view of the large range of temperature covered in this study, for the first time the results should shed light on this latter question.

Shirley has shown that apparent long-range potentials can result from only a nearest-neighbor displacement; as the data in this study were corrected for displacements in a better manner than in previous work, this entire question of an oscillatory potential could be reexamined.

In the previous studies, it was assumed that the dif-

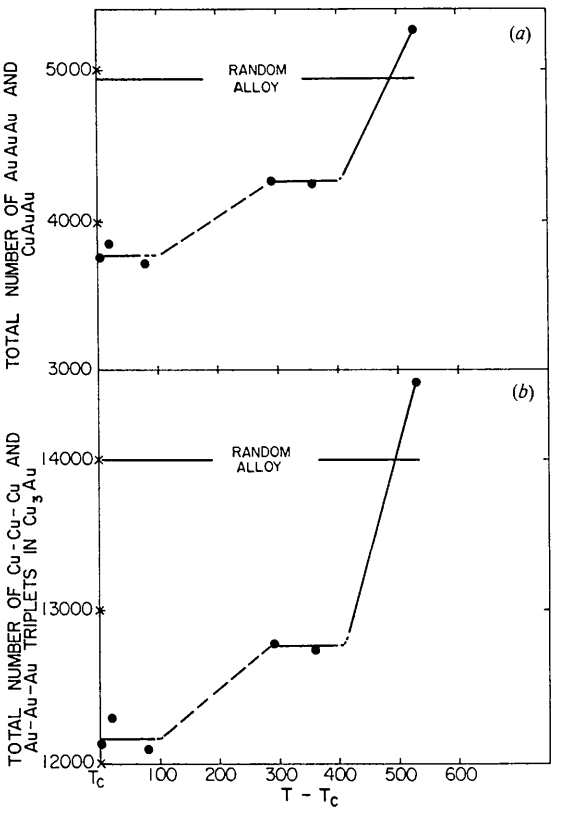

Fig. 10. The total number of (*a*) Au–Au–Au and Cu–Au–Au and (*b*) Au–Au–Au and Cu–Cu–Cu triplets in Cu_3Au obtained from computer simulation as a function of temperature.

Table 9. *Comparison of theoretical and experimental tetrahedron occupation probabilities for* Cu_3Au *as a function of temperature, including Moss's data at* 450 °C

The experimental values, I, refer to the results of the computer simulations; the theoretical values, II, are from Golosov, Popov & Pudan (1973).

	396 °C ($T/T_c=1{\cdot}002$)		420 °C ($T/T_c=1{\cdot}04$)		475 °C ($T/T_c=1{\cdot}12$)	
P	I	II	I	II	I	II
CuCuCuCu	0·2372	0·182	0·2430	0·1870	0·2335	0·1920
CuCuCuAu	0·5463	0·6360	0·5389	0·6320	0·5536	0·6228
CuCuAuAu	0·1962	0·1746	0·1948	0·1752	0·1928	0·1800
CuAuAuAu	0·0186	0·0044	0·0216	0·0049	0·0194	0·0058
AuAuAuAu	0·0011	$0{\cdot}0000_1$	0·0016	$0{\cdot}0000_1$	0·0006	$0{\cdot}0000_1$

	685 °C ($T/T_c=1{\cdot}44$)		750 °C ($T/T_c=1{\cdot}56$)		930 °C ($T/T_c=1{\cdot}80$)		450 °C ($T/T_c=1{\cdot}09$)	
P	I	II	I	II	I	II	I*	II
CuCuCuCu	0·2676	0·2120	0·2615	0·2175	0·2253	0·2273	0·1530	0·1906
CuCuCuAu	0·4948	0·5846	0·5041	0·5760	0·3965	0·5560	0·6970	0·6240
CuCuAuAu	0·2085	0·1932	0·2081	0·1965	0·2070	0·2015	0·1470	0·1798
CuAuAuAu	0·0283	0·0087	0·0253	0·0110	0·0550	0·0127	0·0030	0·0054
AuAuAuAu	0·0009	$0{\cdot}0000_5$	0·0009	$0{\cdot}0000_6$	0·0061	0·0001	0·0000	$0{\cdot}0000_1$

* Moss (1964).

fuse scattering and superlattice reflections occurred in the same location in reciprocal space, in order to obtain a relationship between the critical temperature and the pair potentials, and thereby to reduce the equations to relationships involving ratios of pair potentials V_i/V_1. In view of the various chemical fluctuations reported here, this was not deemed appropriate. Instead we proceeded as follows: The basic equation for determining pair potentials between sites i and j from local order parameters is in the form:

$$f(\alpha_{0j})=2\beta \sum_i V_{ij}\alpha_{0j} \qquad (15)$$

where $\beta=1/kT$. In the Cowley approximation (1950*b*):

$$f(\alpha_{0i})=\ln\left[\frac{(X_A+X_B\alpha_{0i})\,(X_B+X_A\alpha_{0i})}{X_AX_B(1-\alpha_{0i})^2}\right]. \qquad (16a)$$

A lower (linear) approximation was developed by Clapp & Moss (1966):

$$f(\alpha_{0i})=\frac{\alpha_{0i}}{X_AX_B}. \qquad (16b)$$

Least-squares fits were obtained to both equations minimizing the function:

$$F=\sum_{i=1}^{14} W_i[f(\alpha_{0i})_{\text{expt}}-f(\alpha_{0i})_{\text{calc}}]^2 \qquad (17)$$

where W_i is a weighting function. Paskin (1964) has pointed out that the most important information on any oscillation potential is contained in the higher-order α's. Fortunately, these are the ones most precisely obtained in this study. To take into account the errors in the α's, the value chosen for W_1 and W_2 was 0·05. Also, $W_3=0{\cdot}2=W_4$. For the rest of the terms, unit weighing was employed. The fitting procedure was carried out with increasing number of terms up to 14. Surprisingly, the Cowley and the Clapp & Moss approximations gave the same results to within 5–10%, even at 396° close to T_c.

Some caution is necessary in considering the results of such a procedure, because as terms are added, large changes can occur in the potentials. In general it was found that such changes always occur beyond V_7–V_{10}. Accordingly all results reported here are confined to sets involving up V_8.

Table 10. *The nearest-neighbor interatomic energy* NV_1 *in* cal/g-atom *in* Cu_3Au – *a comparison with other calculations*

T°C	Present work	Other work	References
396	856		
405		711	Cowley (1950*b*)
		811	Fournet (1953)
		1040	Moss (1964)
420	841		
475	551		
685	537		
750	692		
930	103		

The values of V_1 at each temperature are given in Table 10 where the values of some other such studies are also presented. At least between the transitions, there is clearly a decrease in the first-neighbor pair potential with increasing temperature. The ratios of pair potentials are given as points for each temperature in Fig. 11(*a*)–(*f*). The curves were obtained from a least-squares fit to the Friedel oscillation:

$$\frac{V_n}{V_1}=\frac{A}{r_{lmn}^3}\cos\left[4{\cdot}911\,(e/a)^{1/3}r_{lmn}+\varphi\right] \qquad (18)$$

where e/a is the electron/atom ratio and r_{lmn} is the interatomic distance for atoms separated by the vector lmn. The term A is a constant and φ is a phase factor. The values of these quantities from this fit are given in Table 11. Disregarding the result at 930 °C, the average value of $e/a=0{\cdot}97$ is in surprisingly good agreement with the value of $1{\cdot}00\pm0{\cdot}03$ obtained by Sato & Toth (1962) from studies of long-period superlattices in the Cu–Au system.

Table 11. *Parameters of the Friedel potential fitted to the data for* Cu_3Au *at various temperatures*

T°C	A	e/a	φ
396	3·042	0·973	1·515
420	3·329	1·002	−1·299
475	3·630	1·002	−1·000
685	2·778	0·965	−0·278
750	2·846	0·917	1·097
930	22·444	1·154	−2·293

The fit of the potentials to an oscillatory potential of the form described by Friedel is only fair. It is worth noting that $V_2/V_1\simeq-0{\cdot}22$ fits the data up to 750 °C, and that this value is the same as that found by Clapp & Moss from Moss's data. Wilkins, employing the same data found the ratio to be −0·18. Even though there are large differences in the α's between our data and Moss's, the ratios of α's are quite similar for large lmn.

Finally, in Fig. 12, the ratios of V's at each temperature are superimposed on the regions of phase stability calculated by Clapp & Moss (1968). It is interesting to note that at most temperatures the system is near the boundary of stability between the $L1_2$ (Cu_3Au) and DO_{22} phases, which probably accounts for the presence of both types of fluctuations.

Conclusions

(1) Short-range order parameters have been obtained from 2° above T_c to 930 °C (near the melting point) after correcting the diffuse intensity for effects due to atomic displacements more fully than heretofore.

(2) The interatomic potentials fit a Friedel oscillation, but only approximately.

(3) The previously disputed specific heat anomalies in Cu_3Au (well above T_c at 600 and 850 °C) have been correlated with changes in local atomic arrangements.

(4) From the total diffuse intensity, computer simu-

lations and interatomic potentials derived from the short-range order parameters, it appears that the anomaly at 600 °C is a disappearance of DO_{22}-like fluctuations in the short-range ordered state, whereas the anomaly at 850 °C is due to the development of CuPt-like regions.

(5) There are premonitory effects just above the critical temperature (T_c) for Cu_3Au; there is a large increase in the Debye–Waller factor, a corresponding increase in the total diffuse intensity due to quadratic terms in atomic displacements, and an apparent change in sign of the average first-neighbor displacements.

We gratefully acknowledge that this research was supported by a grant from the National Science Foundation. Portions of this research were submitted (by P.B.) in partial fulfillment of the requirements for the Ph.D. degree at Northwestern University. Mr W. Schlosberg provided valuable assistance with the operation of the computer programs for control and analysis, and Mr J. Hahn helped immensely with the construction and repair of equipment. Professors L. Schwartz and D. De Fontaine, and Dr E. Epperson reviewed the manuscript. Dr C. Walker offered valuable comments.

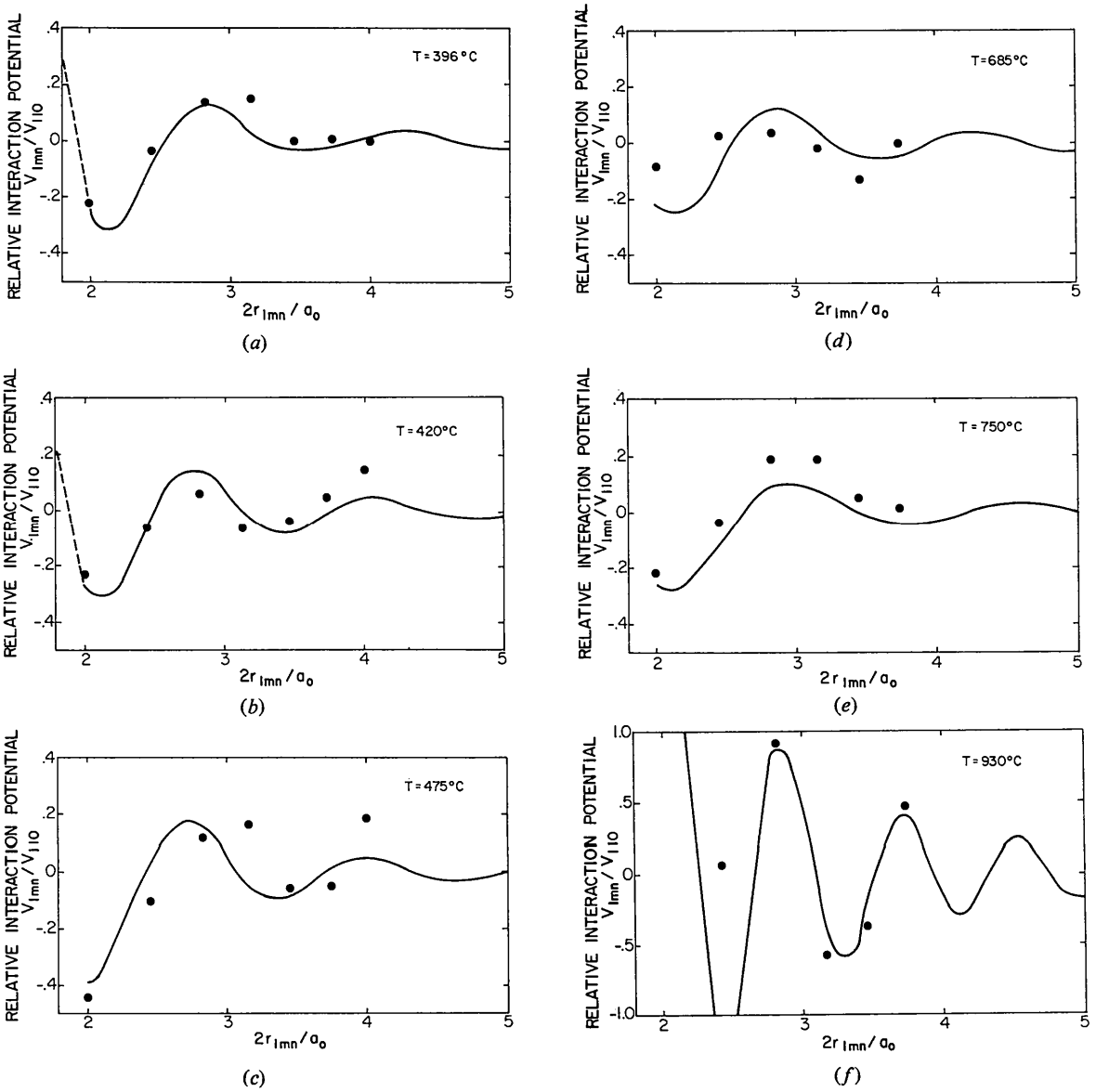

Fig. 11. Relative interaction potentials, V_n/V_1, in Cu_3Au: (*a*) 396 °C, (*b*) 420 °C, (*c*) 475 °C, (*d*) 685 °C, (*e*) 750 °C, (*f*) 930 °C. The fitted Friedel oscillation is also shown as a full line. (Interatomic distance is in units of $2r_{lmn}/a_0$).

References

ASHCROFT, N. W. (1972). *Interatomic Potentials and Simulation of Lattice Defects*, p. 91. New York: Plenum Press.

BATTERMAN, B. W., DE MARCO, J. J. & WEISS, R. J. (1961). *Phys. Rev.* **122**, 68–74.

BENCI, S., GASPARRINI, G. & GERMAGNOLI, E. (1964). *Nuovo Cim.* **31**, 1615–1175.

BERG, H., TSONG, T. T. & COHEN, J. B. (1973). *Acta Metall.* **21**, 1589–1599.

BIDWELL, L. R., SCHULZ, W. J. & SAXER, R. K. (1967). *Acta Metall.* **15**, 1143–1151.

BORIE, B. & SPARKS, C. J. (1971). *Acta Cryst.* A**27**, 198–201.

BORIE, B. & WARREN, B. E. (1956). *J. Appl. Phys.* **27**, 1562–1563.

CLAPP, P. C. & MOSS, S. C. (1966). *Phys. Rev.* **142**, 418–427.

CLAPP, P. C. & MOSS, S. C. (1968). *Phys. Rev.* **171**, 754–763.

COMPTON, A. H. & ALLISON, S. K. (1935). *X-rays in Theory and Experiment*. New York: Van Nostrand.

COOK, H. E. (1974). *J. Appl. Cryst.* **8**, 132–139.

COOPER, M. J. (1963). *Acta Cryst.* **16**, 1067–1069.

COWLEY, J. M. (1950*a*). *J. Appl. Phys.* **21**, 24–30.

COWLEY, J. M. (1950*b*). *Phys. Rev.* **77**, 669–675.

DAMASK, A. C., FUHRMAN, Z. A. & GERMAGNOLI, E. (1961). *J. Phys. Chem. Solids.* **19**, 265–280.

DE FONTAINE, D. (1976). To be published.

DE MARCO, J. J. (1967). *Phil. Mag.* **15**, 483–495.

DOYLE, P. A. & TURNER, P. S. (1968). *Acta Cryst.* A**24**, 390–397.

DUGDALE, R. (1956). *Phil. Mag.* **1**, 537–559.

FEDER, R. & NOWICK, A. S. (1955). *Phys. Rev.* A**98**, 1152.

FOURNET, G. (1953). *J. Phys. Radium*, **14**, 226–234.

FREEMAN, A. J. (1959). *Acta Cryst.* **12**, 261–271; 274–279.

FRIEDEL, J. (1954). *Advanc. Phys.* **3**, 446–507.

GEHLEN, P. C. & COHEN, J. B. (1965). *Phys. Rev.* **139**, A844–A855.

GOLOSOV, N. S. & DUDKA, B. V. (1973). *Phys. Stat. Sol.* (*b*), **59**, 361–366.

GOLOSOV, N. S., POPOV, L. E. & PUDAN, L. YA. (1973). *J. Phys. Chem. Solids*, **34**, 1149–1156; 1157–1163.

GRAGG, J. E., BARDHAN, P. & COHEN, J. B. (1971). *Critical Phenomena in Alloys, Magnets and Superconductors*, pp. 309–337. New York: McGraw-Hill.

GRAGG, J. E. & COHEN, J. B. (1971). *Acta Metall.* **19**, 507–519.

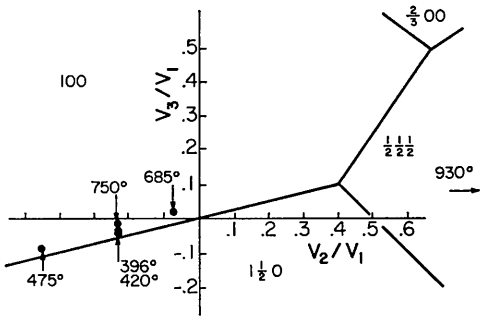

Fig. 12. Minima in $V(k)$ for V_2/V_1 and V_3/V_1 as calculated by Clapp & Moss (1968) for a disordered face-centered cubic lattice with positive V_1. The indices indicate the strongest feature of the diffuse scattering characteristic of that structure: 100 – $L1_2$ (Cu_3Au); $1\frac{1}{2}0$ – DO_{22}; $\frac{1}{2}\frac{1}{2}\frac{1}{2}$ – $L1_1$ (CuPt-like).

GRAGG, J. E., HAYAKAWA, M. & COHEN, J. B. (1973). *J. Appl. Cryst.* **6**, 59–66.

GUARINI, G. & SCHIAVINI, G. M. (1965). *J. Appl. Phys.* **36**, 1719–1720.

GUINIER, A. & GRIFFOUL, R. (1948). *Rev. Metall.* **45**, 387–396.

GUTTMAN, L. (1955). *Solid State Physics, Order–Disorder Phenomena in Metals*, p. 91. London: Academic Press.

HANSON, H. P., HERMAN, F., LEA, J. E. & SKILLMAN, S. (1964). *Acta Cryst.* **17**, 1040–1044.

HASHIMOTO, S. & OGAWA, S. (1970). *J. Phys. Soc. Japan.* **29**, 710–721.

HAYAKAWA, M., BARDHAN, P. & COHEN, J. B. (1975). *J. Appl. Cryst.* **8**, 87–95.

HIRABAYASHI, H., NAGASAKI, S. & KONO, N. (1957). *J. Appl. Phys.* **28**, 1070–1071.

HUANG, K. (1947). *Proc. Roy. Soc.* A**190**, 102–117.

International Tables for X-ray Crystallography (1969). Vol. III. Birmingham: Kynoch Press.

JAARVINEN, M., MERISALO, M. & INKINEN, O. (1969). *Phys. Rev.* **178**, 1108–1110.

JAMES, R. W. & BRINDLEY, G. W. (1931). *Phil. Mag.* **12**, 81–112.

KEATING, D. T. & VINEYARD, G. H. (1956). *Acta Cryst.* **9**, 895–896.

KUCZYNSKI, G. C., DOYAMA, M. & FINE, M. E. (1956). *J. Appl. Phys.* **27**, 651–655.

MARCINKOWSKI, M. J. & ZWELL, L. (1963). *Acta Metall.* **11**, 373–390.

MASUMOTO, H., SAITO, M. & SERGIHARA, H. (1952). Science Rep., Res. Inst., Tohoku Univ., Ser. A4, 482.

MILBERG, M. E. (1958). *J. Appl. Phys.* **29**, 64–65.

MOSS, S. C. (1964). *J. Appl. Phys.* **35**, 3547–3553.

MOSS, S. C. (1965). *Local Atomic Arrangements Studied by X-ray Diffraction*, pp. 95–122. New York: Gordon & Breach.

MOSS, S. C. (1969). *Phys. Rev.* **22**, 1108–1111.

MOSS, S. C. & CLAPP, P. C. (1968). *Phys. Rev.* **171**, 764–777.

OHSHIMA, K. & WATANABE, D. (1973). *Acta Cryst.* A**28**, 520–526.

OWEN, E. A. & EVANS, E. W. (1967). *Brit. J. Appl. Phys.* **18**, 605–609.

PAAVOLA, K., RICHESSON, M., MORRISON, L. & COHEN, J. B. (1971). *J. Appl. Cryst.* **4**, 524–527.

PASKIN, A. (1964). *Phys. Rev.* **134**, A246–A249.

RAETHER, H. (1952). *Z. angew. Phys.* **4**, 53–59.

SATO, H. & TOTH, R. S. (1962). *Phys. Rev. Lett.* **8**, 239–241.

SCHÜLE, W. (1957). Ph. D. Thesis, Max Planck Inst. für Metall., Stuttgart.

SCHWARTZ, L. H. & COHEN, J. B. (1965). *J. Appl. Phys.* **36**, 598–616.

SCHWARTZ, L. H., MORRISON, L. A. & COHEN, J. B. (1963). *Advanc. X-ray Analysis*. Vol. 7. New York: Plenum Press.

SHIRLEY, C. G. (1974). *Phys. Rev.* **10**, B1149–B1159.

SINCLAIR, R. & THOMAS, G. (1975). *J. Appl. Cryst.* **8**, 206–210.

SIEGEL, S. (1940). *Phys. Rev.* **57**, 537–545.

SPARKS, C. J. & BORIE, B. (1965). *Local Atomic Arrangements Studied by X-ray Diffraction*, pp. 5–50. New York: Gordon and Breach.

STRONG, S. & KAPLOW, R. (1967). *Acta Cryst.* **23**, 38–44.

SUORTTI, P. (1972). *J. Appl. Cryst.* **5**, 325–331.

TAGGART, G. B. & TAHIR-KHELI, R. A. (1973). *Physica* **68**, 93–106.

TAHIR-KHELI, R. A. (1969). *Phys. Rev.* **188**, 1142–1153.

TANNER, L. (1968). Tech. Note 33, Ledgemont Laboratory, Kennecott Copper Corporation, Lexington, Massachusetts.
TANNER, L., CLAPP, P. C. & TOTH, R. S. (1968). *Mater. Res. Bull.* **3**, 855–861.
TIBBALLS, J. E. (1974). Ph. D. Thesis, Univ. of Melbourne, Melbourne.
TOWERS, G. R. (1972). Ph.D. Thesis, Univ. of Melbourne, Melbourne.
WALKER, C. B. & CHIPMAN, D. R. (1970). *Acta Cryst.* A**26**, 447–455.
WALKER, C. B. & KEATING, D. T. (1963). *J. Appl. Phys.* **34**, 2309–2312.
WARREN, B. E., AVERBACH, B. L. & ROBERTS, B. W. (1951). *J. Appl. Phys.* **22**, 1493–1496.
WARREN, B. E. & MOZZI, R. L. (1966). *Acta Cryst.* **21**, 459–461.
WILCHINSKY, Z. W. (1944). *J. Appl. Phys.* **15**, 806–812.
WILKINS, S. (1970). *Phys. Rev.* **2**, B3935–B3942.
WILLIAMS, R. O. (1970). Oak Ridge National Laboratory Report ORNL-TM-2866.
WOLFF, P. M. DE (1956). *Acta Cryst.* **2**, 682–683.

Acta Cryst. (1976). A**32**, 614

A Restrained-Parameter Structure-Factor Least-Squares Refinement Procedure for Large Asymmetric Units

BY JOHN H. KONNERT

Laboratory for the Structure of Matter, Naval Research Laboratory, Washington, D.C., 20375, U.S.A.

(*Received* 2 *September* 1975; *accepted* 27 *October* 1975)

A rapidly converging method for refining approximate atomic models is presented. It combines the conditional structure-factor least-squares procedure described by Waser [*Acta Cryst.* (1963). **16**, 1091–1094] with the conjugate gradient method for solving linear systems [Hestenes & Stiefel, *J. Res. Natl. Bur. Stand.* (1952). **49**, 409–436]. The method allows simultaneous variation of all of the structural parameters, although less than 1% of the derivative matrix need be calculated and stored for large systems and less than $\frac{1}{64}$th of the diffraction data accessible with Cu radiation need be used. Applications involving a 240 atom mineral and an 812 atom protein are mentioned.

Introduction

Approximate atomic models for large structures such as complex minerals and biological macromolecules may be obtained by various means. These methods include consideration of sub-cell symmetry and/or direct methods in the case of complex minerals and isomorphous replacement and anomalous dispersion techniques for macromolecules. The cost of conventional least-squares refinement of these trial structures, which may contain from several hundred to thousands of atoms, is in many cases prohibitive. A notable exception is the refinement of rubredoxin (Watenpaugh, Sieker, Herriott & Jensen, 1973). In some instances, particularly with macromolecules, the intensity data may be too limited. Several alternative approaches have been reported. In the field of protein crystallography, a constrained-model refinement is often employed to give a best fit to an electron-density Fourier map that has been calculated with approximate phases (Diamond, 1971). This model may then be used to compute improved phases from which a new Fourier map may be calculated and the procedure is cycled (Deisenhofer & Steigemann, 1975). Difference Fourier map refinements have also been used (Watenpaugh *et al.*, 1973), and combined with cycles of model idealization (Moews & Kretsinger, 1973; Freer, Alden, Carter & Kraut, 1975). For some minerals, refinement of trial structures employing only distance restraints has proved valuable (Barrer & Villiger, 1969; Meier & Villiger, 1969). These minerals have been of such a size as to permit the models obtained from a least-squares refinement of the distances to be further refined by conventional least squares.

An alternative to these techniques that simultaneously employs both intensity data and distance restraints is presented in this paper. The method is an extension of the conditional structure-factor least-squares technique described by Waser (1963). Subsidiary conditions in this technique are treated as observational equations; *i.e.*, the sum of squared residuals to be minimized is a function of not only observed and calculated intensities, but also ideal and calculated distances. Other subsidiary conditions, such as those involving thermal parameters, may also be included. The extension of the technique utilizes specific properties of the conjugate gradient method for solving linear systems (Hestenes & Stiefel, 1952). Two important features affecting the efficiency of this method are the choice of the elements of the derivative matrix to be retained and the selection of a subset of intensity data. Although less than 1% of the derivative matrix needs to be calculated and stored for large systems, and as little as 1/64th of the intensity data accessible with Cu